Antiparallel microtubule bundling supports KIF15-driven mitotic spindle assembly

Brittany M. Salazar⊙ and Ryoma Ohi*
Department of Cell and Developmental Biology, University of Michigan; Ann Arbor, MI 48109

ABSTRACT The spindle is a bipolar microtubule-based machine that is crucial for accurate chromosome segregation. Spindle bipolarity is generated by Eg5 (a kinesin-5), a conserved motor that drives spindle assembly by localizing to and sliding apart antiparallel microtubules. In the presence of Eg5 inhibitors (K5Is), KIF15 (a kinesin-12) can promote spindle assembly, resulting in K5I-resistant cells (KIRCs). However, KIF15 is a less potent motor than Eg5, suggesting that other factors may contribute to spindle formation in KIRCs. Protein Regulator of Cytokinesis 1 (PRC1) preferentially bundles antiparallel microtubules, and we previously showed that PRC1 promotes KIF15-microtubule binding, leading us to hypothesize that PRC1 may enhance KIF15 activity in KIRCs. Here, we demonstrate that: 1) loss of PRC1 in KIRCs decreases spindle bipolarity, 2) overexpression of PRC1 increases spindle formation efficiency in KIRCs, 3) overexpression of PRC1 protects K5I naïve cells against the K5I S-trityl-L-cysteine (STLC), and 4) PRC1 overexpression promotes the establishment of K5I resistance. These effects are not fully reproduced by a TPX2, a microtubule bundler with no known preference for microtubule orientation. These results suggest a model wherein PRC1-mediated bundling of microtubules creates a more favorable microtubule architecture for KIF15-driven mitotic spindle assembly in the context of Eg5 inhibition.

💡 New Hypothesis

SIGNIFICANCE STATEMENT

- The kinesin-12 (KIF15) can substitute for kinesin-5 (Eg5) during spindle assembly, but KIF15 is less efficient in this role due to its reduced ability to generate microtubule sliding forces. It was hypothesized that microtubule-bundling factors that stabilize antiparallel microtubule overlaps may facilitate KIF15 activity during spindle assembly.

- The authors showed that PRC1, an antiparallel microtubule crosslinking protein, is required for KIF15-dependent spindle assembly, and that its overexpression can promote cancer-cell resistance to K5Is.

- This work has implications for cancer therapies that operate by blocking spindle assembly.

INTRODUCTION

The mitotic spindle is a bipolar microtubule (MT)-based machine that is crucial for accurate chromosome segregation during cell division (McIntosh *et al.*, 1969; Petry, 2016; Oriola *et al.*, 2018; Kapoor, 2017; Valdez *et al.*, 2023). Improper mitotic spindle assembly leads to errors in chromosome segregation, which in turn fuels cellular transformation (Sansregret and Swanton, 2017; Ben-David and Amon, 2020; Baker *et al.*, 2024). The spindle is also a target for antimitotic agents such as the MT-targeting poisons taxol and the vinca alkaloids, drugs that remain important standard-of-care chemotherapies (Janssen and Medema, 2011). MTs are dynamic cylindrical polymers of tubulin which

undergo repeated cycles of polymerization and depolymerization (Mitchison and Kirschner, 1984). MT-targeting poisons are effective as anticancer agents in part because they hinder proper spindle assembly by interfering with MT dynamics, leading to prolonged mitotic arrest and apoptosis (Rowinsky et al., 1990; Jordan et al., 1992; Toso et al., 1993; Janssen and Medema, 2011; Zhang and Kanakkanthara, 2020). However, MT-targeting poisons have unavoidable negative side effects, owing to the broad importance of MTs in both nontransformed proliferative and postmitotic cells. Development of antimitotic drugs that work by mechanisms more specific to cell division is therefore an important goal for cancer research.

In most eukaryotic organisms, spindle assembly is driven by kinesin-5 (Eg5), a homotetrameric motor that slides antiparallel MTs apart (Sawin et al., 1992; Kapoor et al., 2000; Kapitein et al., 2005; Skoufias et al., 2006; Cross and McAinsh, 2014). Accordingly, inhibition of Eg5 by small molecule inhibitors in human cells prevents spindle formation (Mayer et al., 1999) and is thereby cytotoxic (Orth et al., 2008; Shi et al., 2008), making it a potential target for cancer therapy. However, clinical trials have demonstrated that Eg5 inhibitors (K5Is) are not efficacious as cancer drugs (DeBonis et al., 2004; Skoufias et al., 2006; Rath and Kozielski, 2012; Garcia-Saez and Skoufias, 2021). We and others have shown that KIF15 can promote spindle assembly in the absence of Eg5 activity (Tanenbaum et al., 2009; Vanneste et al., 2009; Sturgill and Ohi, 2013; Dumas et al., 2016; Sturgill et al., 2016), suggesting that drug resistance may underlie the ineffectiveness of K5Is. To understand how human cells evade the cytotoxic effects of K5Is, we have studied spindle assembly mechanisms in cells experimentally adapted to live in the presence of K5Is (KIRCs) as well as the biophysical properties of KIF15.

In vitro, KIF15 is similar to Eg5 in that it slides antiparallel MTs apart, providing an explanation for how KIF15 is able to substitute for Eg5 during spindle assembly (Tanenbaum et al., 2009; Vanneste et al., 2009; Dumas et al., 2016; Sturgill et al., 2016; Reinemann et al., 2017; Milic et al., 2018). However, unlike Eg5, the force that KIF15 generates within an overlap region does not scale with motor number (Reinemann et al., 2017; Shimamoto and Kapoor, 2018), and it is perhaps for this reason that KIF15 is not an efficient spindle assembly motor (Sturgill and Ohi, 2013; Sturgill et al., 2016). Moreover, KIF15 does not bind individual MTs efficiently, most likely a consequence of autoinhibition (Sturgill et al., 2014). KIF15 is, however, recruited to MTs bundled by Protein Regulator of Cytokinesis 1 (PRC1; Sturgill et al., 2014), a MT-associated protein (MAP) that preferentially cross-links MTs in antiparallel orientation (Bieling et al., 2010; Subramanian et al., 2010). PRC1 has a central role in stabilizing regions of antiparallel MT overlap within the midzone of cytokinetic cells (Mollinari et al., 2002; Kurasawa et al., 2004; Green et al., 2012; Li et al., 2021b) and has recently been found to stabilize the bridging fibers of bioriented chromosomes at the metaphase plate (Kajtez et al., 2016; Matkovic et al., 2022; Renda et al., 2022). Interestingly, in vitro reconstitution studies have shown that PRC1 can resist and modulate forces exerted within regions of antiparallel MT overlap (Bieling et al., 2010; Subramanian et al., 2010; Gaska et al., 2020; Alfieri et al., 2021). In this work, we test the hypothesis that PRC1 may facilitate KIF15 activity during spindle assembly in K5I-resistant cells (KIRCs), and address the possibility that PRC1 may promote resistance to K5Is. We also demonstrate that the geometry of MT bundles may be important for circumventing Eg5 inhibition and shifting to KIF15-driven mitotic spindle assembly.

RESULTS

PRC1 is present on the preanaphase mitotic spindle

Motivated by our previous observation that KIF15-MT binding is strongly enhanced by PRC1-mediated MT bundling in vitro (Sturgill et al., 2014), we analyzed the localization of PRC1 during metaphase in KIRCs. We used two sets of K5I-naïve cells and an associated KIRC: TP53⁻/⁻ RPE-1 (hereafter RPE-1; Izquierdo et al., 2014) and its K5I-resistant derivative KIRC-1 (hereafter RPE-1 KIRC-1; Dumas et al., 2019) and HeLa cells that stably express EB3-GFP (hereafter HeLa^EB3-GFP) and a derived KIRC (hereafter HeLa KIRC^EB3-GFP; see Materials and Methods). We confirmed that HeLa KIRC^EB3-GFP does not rely on Eg5 for mitotic spindle assembly by RNAi (Supplemental Figure S1B) but does rely on KIF15, as is the case with other KIRCs that we and others have described previously (Dumas et al., 2016; Sturgill et al., 2016).

To examine PRC1 localization during mitosis, we performed immunostaining using a new PRC1 antibody that we generated (see Materials and Methods). Our motivation to raise a new antibody against PRC1 was that emerging work highlights a role for this MAP during metaphase (Polak et al., 2017; Jagric et al., 2021; Matkovic et al., 2022; Renda et al., 2022), but commercial antibodies decorate MTs predominantly during cytokinesis (Li et al., 2021b). On immunoblots, our antibodies recognize two bands of ~71 kDa (Figure 1, C and D), consistent with PRC1 being expressed as two isoforms (Ota et al., 2004). Both bands decrease in intensity upon RNAi of PRC1, indicating that the antibodies are PRC1-specific (Figure 2B). Moreover,
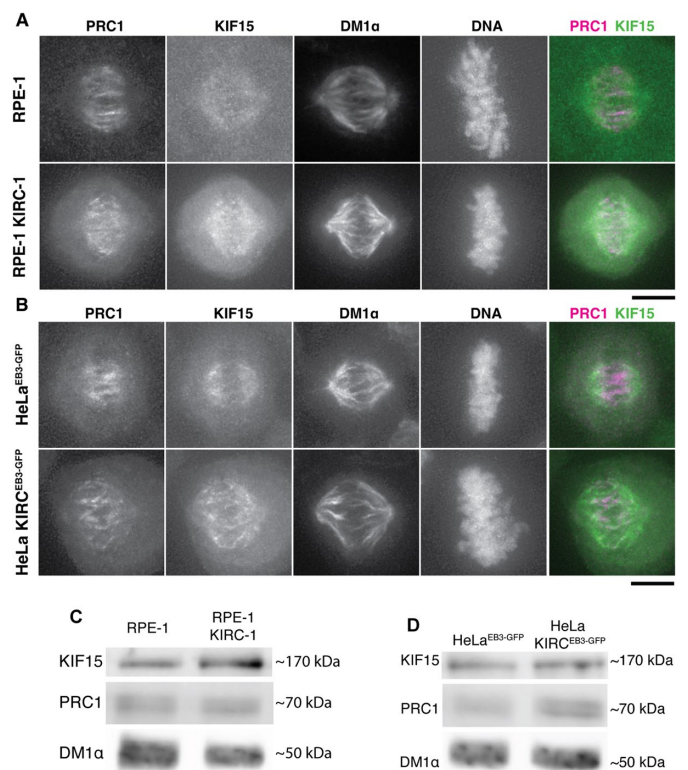
FIGURE 1: PRC1 localizes to the preanaphase mitotic spindle. (A) PRC1 and KIF15 localization in fixed RPE-1 (upper row) and RPE-1 KIRC-1 cells as shown by immunofluorescence microscopy. (B) PRC1 and KIF15 localization in fixed HeLa^EB3-GFP (upper row) and HeLa KIRC^EB3-GFP cells as shown by immunofluorescence microscopy. In all micrographs, tubulin was detected using the DM1α antibody, DNA by Hoechst 33342. Scale bars, 10 μm. (C and D) Immunoblots of KIF15, PRC1 and tubulin (DM1α) using lysates from the indicated cell lines.
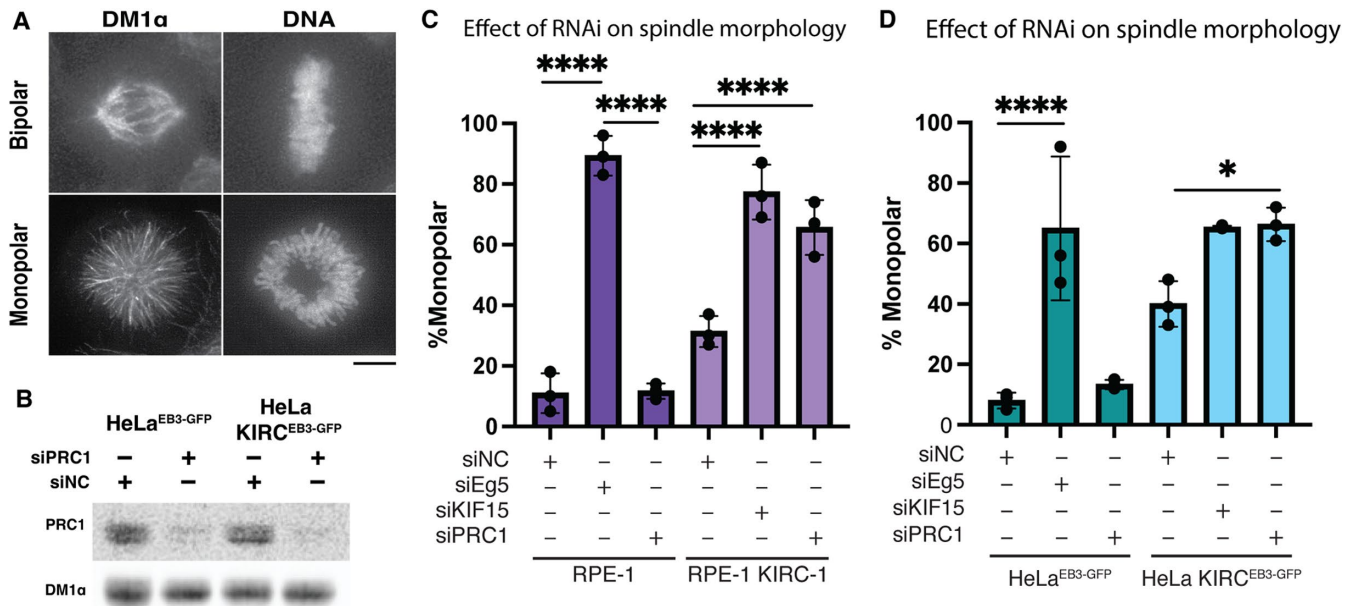
FIGURE 2: PRC1 depletion impairs bipolar spindle assembly in KIRCs. (A) Representative maximum z projection micrographs of bipolar and monopolar spindles in RPE-1 cells. Tubulin was detected using DM1α, DNA with Hoechst 33342. Scale bar, 10 µm. (B) Immunoblot showing PRC1 levels in HeLa[EB3-GFP] and HeLa KIRC[EB3-GFP] transfected with the indicated siRNAs. Tubulin was detected using DM1α. (C and D) Quantitation of the percentage of monopolar spindles upon RNAi of the indicated genes in RPE-1 and RPE-1 KIRC-1 (C), HeLa[EB3-GFP] and HeLa KIRC[EB3-GFP] (D) as evaluated by in fixed cells. Bars indicate mean of three biological replicates, dots indicate percentage for each replicate, $n = 300$ per group, error bars indicate SD, significance was calculated by two-way ANOVA, * $p = 0.0399$, **** $p < 0.0001$.

immunoblots of cell lysates containing PRC1 fused to mCherry show a slower migrating band (Figure 3F). By immunostaining, we observed that PRC1 is present on the metaphase spindle of RPE-1 and HeLa[EB3-GFP] cells, as well on the metaphase spindles of their associated KIRCs (Figure 1, A and B). Qualitatively, PRC1 localization appears to be enhanced on the spindle equator of some KIRCs, although a consistent difference in localization between parental and KIRCs could not be quantified (Figure 1, A and B). As previously described (Dumas *et al.*, 2019), we find that KIF15 is enriched on the metaphase spindles of RPE-1 KIRC-1 cells, and also on metaphase spindles of HeLa KIRC[EB3-GFP] cells (Figure 1, A and B). Eg5 is absent from the metaphase spindles of both KIRCs (Supplemental Figure S1, A and B).

### Knockdown of PRC1 impairs bipolar spindle assembly in KIRCs

To determine whether PRC1 is important for spindle assembly in KIRCs, we depleted PRC1 by RNAi. Transfection of cells with PRC1 siRNAs, but not control siRNAs, reduced PRC1 protein levels in cells, as assessed by immunoblotting (Figure 2B) and immunofluorescence (Supplemental Figure S2, A and B). Upon knockdown of PRC1, both RPE-1 KIRC-1 and HeLa KIRC[EB3-GFP] exhibit an increased percentage of monopolar spindles (RPE-1 KIRC-1: siNC, 68.7% bipolar to 31.3% monopolar, $n = 300$, compared with siPRC1 22.7% bipolar to 77.3% monopolar, $n = 300$; HeLa KIRC[EB3-GFP]: siNC, 60% bipolar to 40% monopolar, $n = 300$, compared with siPRC1 33.7% bipolar to 66.3% monopolar, $n = 300$), indicating that loss of PRC1 prevents proper bipolar spindle assembly in KIRCs. Interestingly, depletion of PRC1 disabled spindle formation in KIRCs to a similar extent as depletion of KIF15 (Figure 2, C and D), which would be consistent with the two proteins working in the same spindle assembly pathway. In contrast, loss of PRC1 in RPE-1 and HeLa[EB3-GFP] cells had no impact on spindle assembly, but led to the formation of binucleate cells, as expected from previous work (Mollinari *et al.*, 2002). These results

indicate that the importance of PRC1 during spindle assembly is specific to KIRCs.

PRC1 overexpression rescues mitotic delay in HeLa KIRC[EB3-GFP] cells

We next sought to determine how overexpression of PRC1 affects the progression of KIRCs through mitosis. We first characterized the kinetics of mitosis in RPE-1, HeLa[EB3-GFP], RPE-1 KIRC-1, and HeLa KIRC[EB3-GFP] cells. Given the demonstrated reduced MT sliding efficiency of KIF15 compared with Eg5 in in vitro studies (Reinemann *et al.*, 2017) and previous characterization of KIRCs in our lab (Sturgill and Ohi, 2013), we speculated that the spindle assembly kinetics of KIRCs may be affected compared with parental cells. On average, the parental cell lines progressed from nuclear envelope breakdown (NEB) to metaphase, defined as the time point where the majority of chromosomes were visualized aligned at the metaphase plate by DIC microscopy, in 16.67 ± 5.31 min for RPE-1 (mean ± SD, $N = 30$) and 24.83 ± 9.33 min for HeLa[EB3-GFP] (mean ± SD, $n = 30$; Figure 3, A and B, quantified in C). In these cell lines, anaphase occurred within 41.83 ± 18.64 (RPE-1, $n = 30$) and 55 ± 11.6 min (HeLa[EB3-GFP], $n = 30$; Figure 3D). Both of these measurements were significantly lengthened in KIRCs. RPE-1 KIRC-1 and HeLa KIRC[EB3-GFP] cells reached metaphase within 33.67 ± 13.64 ($n = 30$) and 63 ± 18.64 20.97 ($n = 30$) min, respectively (Figure 3, A, B, and C; Supplemental Video S1). These KIRCs underwent anaphase in 67.33 ± 26.71 (RPE-1 KIRC-1, $n = 30$) and 116.7 ± 36.47 min (HeLa KIRC[EB3-GFP], $n = 30$), respectively (Figure 3D).

We then tested whether overexpression of PRC1 could rescue mitotic delay in HeLa KIRC[EB3-GFP] cells. We focused on this cell line because it transfects more readily than RPE-1 and RPE-1 KIRC-1 cells and the EB3-GFP tag allows for observation of MT dynamics and centrosome separation. PRC1-mCherry was introduced into HeLa[EB3-GFP] and HeLa KIRC[EB3-GFP] cells by transient transfection, and
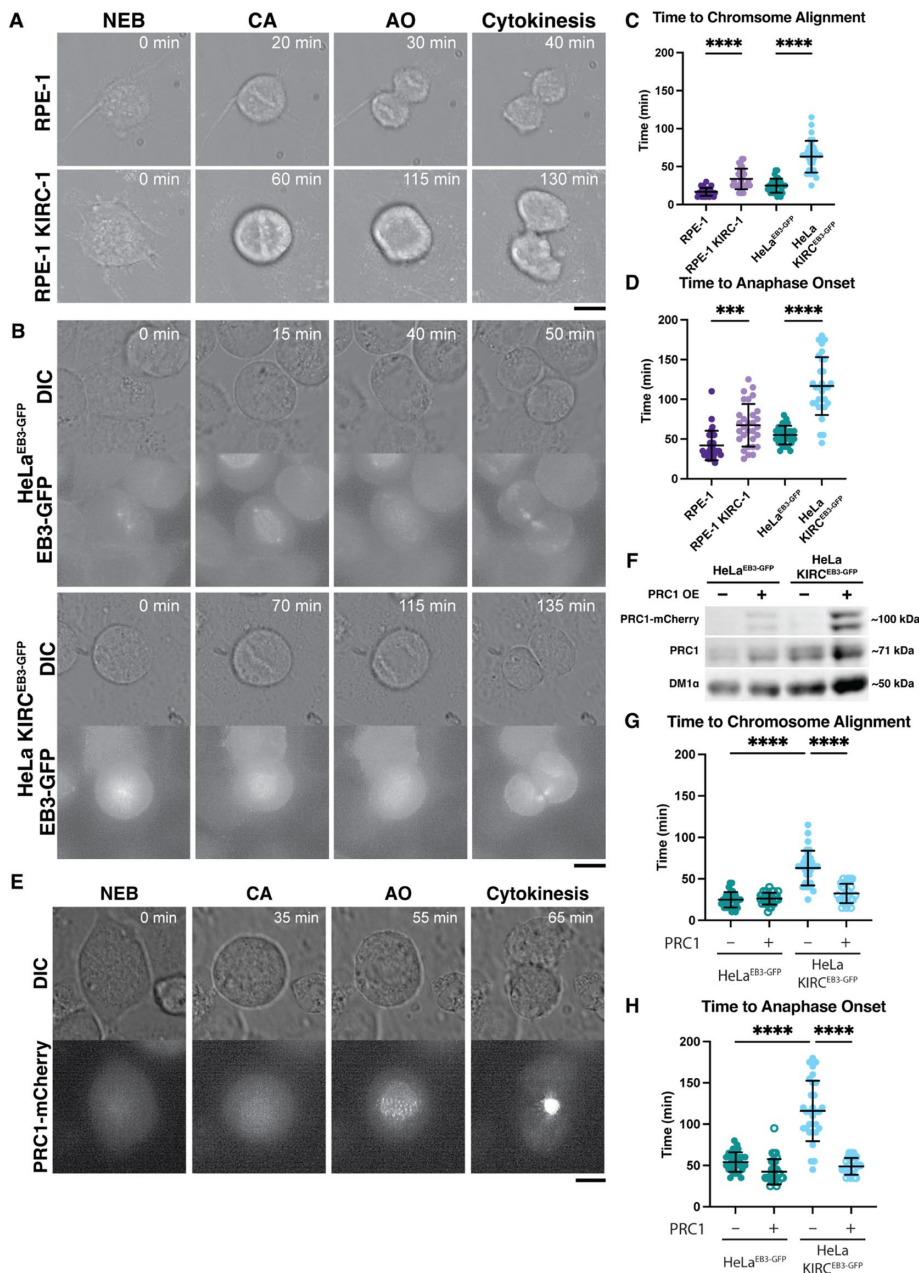
FIGURE 3: KIRCs experience a delay in progression through mitosis that is rescued by PRC1 overexpression. For micrographs in (A), (B), and (E), live cells were imaged every 5 min for 90–190 min. Micrographs in A) show NEB, chromosome alignment (CA), anaphase onset (AO), and cytokinesis time points for RPE-1 (upper row) and RPE-1 KIRC-1 (lower row) by DIC. Micrographs in B) show timing of the same events for HeLa[EB3-GFP] (upper double row) and HeLa KIRC[EB3-GFP] (lower double row) by DIC and maximum z projection GFP fluorescence microscopy. EB3-GFP was imaged in the GFP channel. (C) Quantification of time needed for chromosome alignment in the indicated cell lines. (D) Quantification of time needed for anaphase onset in the indicated cell lines. Micrographs in E) show NEB, CA, AO, and cytokinesis time points by DIC and maximum z projection mCherry fluorescence microscopy in HeLa KIRC[EB3-GFP] cells that overexpressed PRC1-mCherry. (F) Immunoblots showing protein levels of PRC1 following transient overexpression ("OE") in HeLa[EB3-GFP] and HeLa KIRC[EB3-GFP]. (G and H) Quantification of time needed for chromosome alignment (G) and anaphase onset (H) for HeLa[EB3-GFP] and HeLa KIRC[EB3-GFP] cells with or without PRC1-mCherry overexpression. For all graphs, dots represent individual cells, unfilled circles indicate PRC1-mCherry overexpression, bars indicate mean and SD, $n = 30$ per cell line, >three biological replicates. Significance was calculated by ordinary one-way ANOVA, **** $p < 0.0001$. Scale bars, 10 μm.

the cells were imaged by time-lapse mCherry fluorescence and DIC microscopy (Figure 3E, Supplemental Video S2). We then quantified the time required for cells to progress from NEB to metaphase and anaphase onset. Strikingly, overexpression of PRC1 rescued the time required for HeLa KIRC[EB3-GFP] to reach metaphase (32.00 ± 11.57 min, $n = 30$) and initiate anaphase (51.67 ± 12.27 min, $n = 30$; Figure 3, G and H). PRC1 overexpression did not affect mitotic progression in HeLa[EB3-GFP] cells (Figure 3, G and H).

PRC1 facilitates KIF15-driven spindle assembly in the presence of an Eg5 rigor mutant

We showed previously that HeLa-derived KIRC-2 cells express an Eg5 rigor mutant (G268V) that is essential for KIF15-dependent spindle assembly in this cell line. This Eg5 mutant may facilitate spindle assembly by bundling MTs, thereby creating preferred MT substrates for KIF15 (Sturgill *et al.*, 2016). Because our data suggest a similar role for PRC1 in promoting KIF15 activity, that is, bundling MTs, we wanted to test whether PRC1 is also required in HeLa KIRC-2 cells.

Similar to RPE-1 KIRC-1 and HeLa KIRC[EB3-GFP] cells, PRC1 is present on the metaphase spindle in HeLa and HeLa KIRC-2 cells, while KIF15 is enriched on HeLa KIRC-2 spindles compared with parental spindles (Figure 4A). We depleted PRC1 in HeLa and HeLa KIRC-2 cells by RNAi, and found that PRC1 knockdown impairs bipolar spindle assembly in HeLa KIRC-2 cells, but not HeLa cells (HeLa: siNC, 83.7% bipolar to 16.3% monopolar, $n = 300$, compared with siPRC1 74.7% bipolar to 25.3% monopolar, $n = 300$; HeLa KIRC-2: siNC, 58.7% bipolar to 41.3% monopolar, $n = 300$, compared with siPRC1 21.3% bipolar to 78.7% monopolar, $n = 300$; Figure 4C). This result demonstrates that PRC1 is important for KIF15-driven spindle assembly, even in the presence of the Eg5 rigor mutant. By live-cell imaging, we further determined that HeLa KIRC-2 cells display a delay in progression through mitosis compared with parental HeLa cells (average time to chromosome alignment 60.83 min and 26.00 min, respectively, average time to anaphase onset 106.7 min and 52.00 min, respectively; Figure 4, D, G, and H). These defects in mitotic timing could be rescued by overexpression
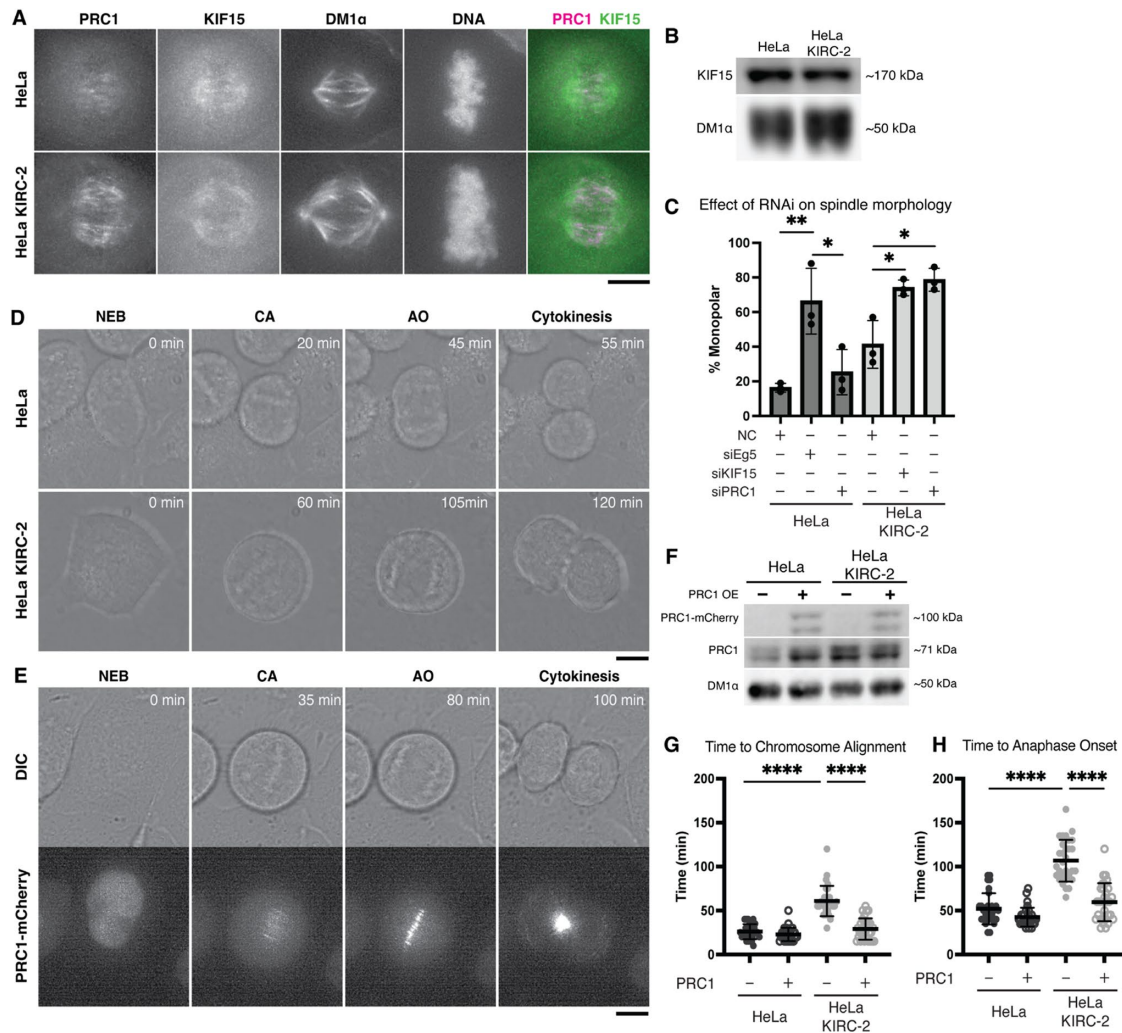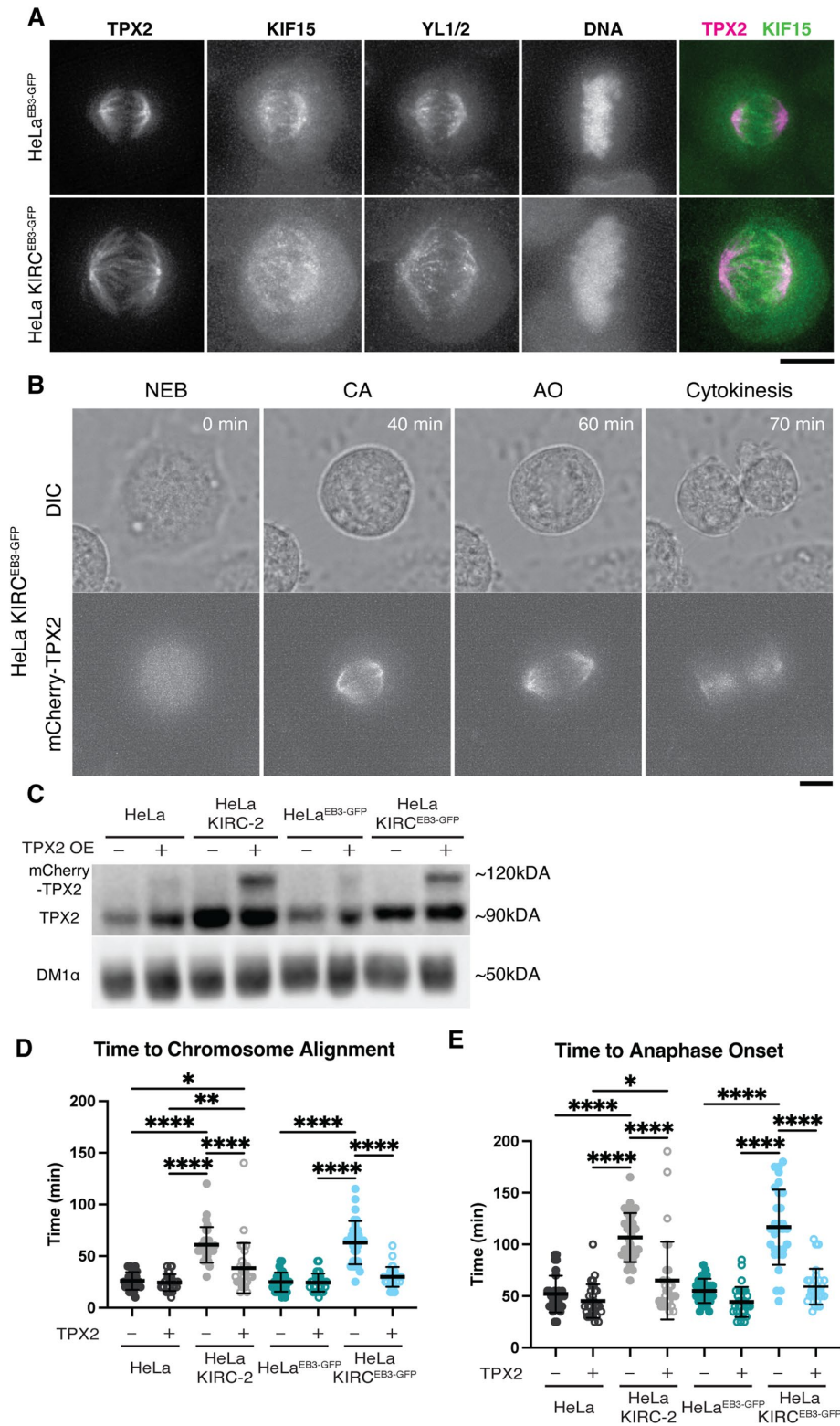
FIGURE 4: PRC1 promotes KIF15-driven spindle assembly in the presence of an Eg5 rigor mutant. (A) Representative images showing PRC1 and KIF15 localization in HeLa (upper row) and HeLa KIRC-2 (lower row) cells by immunofluorescence microscopy. Tubulin was detected using DM1α, DNA with Hoechst 33342. (B) Immunoblot of KIF15 and tubulin in lysates prepared from HeLa and HeLa KIRC-2 cells. (C) Quantitation of the percentage of monopolar spindles upon RNAi of the indicated genes in HeLa and HeLa KIRC-2 cells. Bars indicate mean of three biological replicates, dots indicate percentage for each replicate, n = 300 per group, error bars indicate SD, significance was calculated by two-way ANOVA, ** p = 0.0026, * p ≤ 0.0415. Micrographs in (D) and (E) show NEB, CA, AO, and cytokinesis time points in live cells in HeLa (D, upper row) and HeLa KIRC-2 (D, lower row) by DIC, as well as HeLa KIRC-2 cells overexpressing PRC1-mCherry (E) by DIC and maximum z projection mCherry fluorescence microscopy. Cells were imaged every 5 min for 90 to 190 min total. (F) Immunoblots showing levels of PRC1 and PRC1-mCherry overexpression ("OE") in HeLa and HeLa KIRC-2. Tubulin was detected using DM1α. G and H) Quantification of time needed for chromosome alignment (G) and anaphase onset (H) in HeLa and HeLa KIRC-2 cells with and without PRC1-mCherry overexpression. Dots indicate individual cells, unfilled circles indicate PRC1-mCherry overexpression, bars indicate mean and SD, n = 30 cells per group, > three biological replicates, significance was calculated by ordinary one-way ANOVA, **** p < 0.0001. Scale bars, 10 μm.

of PRC1 (Figure 4, E, G, and H). Taken together, these results indicate that PRC1 assists KIF15-driven spindle assembly even in the presence of an Eg5 rigor mutant.

TPX2 rescues spindle assembly delay in KIRCs

We then asked whether another MT bundling factor could rescue spindle assembly in KIRCs. TPX2 is a MT nucleator and bundler that has been found in *Xenopus* to be required for targeting KIF15 to spindle MTs (Wittmann *et al.*, 2000). Unlike PRC1, however, TPX2 has not been reported to bundle MTs in an orientation-dependent manner. In fixed cells at metaphase, TPX2 is localized close to the spindle poles in all cell lines used in this study (Figures 5A; Supple-

mental Figure S4, A and B). To assess the effect of TPX2 on spindle assembly, we overexpressed mCherry-TPX2 in HeLa, HeLa KIRC-2, HeLa[EB3-GFP], and HeLa KIRC[EB3-GFP] and imaged the protein in live cells (Figure 5B; Supplemental Video S3). We observed that TPX2 was able to rescue time to chromosome alignment and anaphase onset in both KIRC lines (HeLa KIRC-2, time to CA with TPX2 overexpression 38.33 ± 24.19 min, AO 65 ± 37.6 min; HeLa KIRC[EB3-GFP], time to CA 29.83 ± 9.6 min, AO 59.17 ± 17.27 min, n = 30 for each cell line; Figure 5, D and E), indicating that TPX2, like PRC1, can support KIF15-driven spindle assembly in KIRCs. Like PRC1, TPX2 overexpression did not affect mitotic progression in parental cell lines.

Transient PRC1 overexpression facilitates spindle assembly during acute inhibition of Eg5

Given the importance of PRC1 in KIF15-driven spindle assembly in our KIRCs, we asked whether transient PRC1 overexpression could protect cells against the detrimental effects of Eg5 inhibition in K5I naïve cells. To test this, HeLa and HeLa[EB3-GFP] cells were transfected with PRC1-mCherry, treated with S-trityl-L-cysteine (STLC) for 3 h, fixed, immunostained, and the percentage of monopolar and bipolar spindle morphologies in only mCherry positive cells were quantified (Figure 6, B and D; Supplemental Figure S5). Compared to a negative control, transient PRC1 overexpression increased the percentage of bipolar spindles after STLC treatment in both cell lines (HeLa: NC, 89.3% monopolar to 10.7% bipolar, PRC1 overexpression 67% monopolar to 33% bipolar; HeLa[EB3-GFP]: NC, 84% monopolar, 16% bipolar, PRC1 overexpression, 59.7% monopolar, 40.3% bipolar; Figure 6D). This result demonstrates that PRC1 overexpression provides a modest degree of protection against STLC treatment in K5I naïve cells.

We then asked whether TPX2 is also able to protect cells against acute inhibition of Eg5 and tested this in the same way described above. In contrast to PRC1, TPX2 overexpression did not affect spindle morphology in either cell line following STLC treatment (HeLa: TPX2 overexpression, 89% monopolar to 11% bipolar; HeLa[EB3-GFP]: TPX2 overexpression, 83.3% monopolar, 16.7% bipolar; Figure 6, C and D). This result suggests that MT geometry is important for overcoming acute STLC challenge in K5I naïve cells.

Stable PRC1 overexpression protects against acute inhibition of Eg5 while TPX2 does not

To test the effects of stable PRC1 and TPX2 overexpression, we established doxycycline inducible PRC1-mCherry and mCherry-TPX2 overexpressing cell lines – hereafter HeLa[PRC1-mCherry] and HeLa[mCherry-TPX2],

FIGURE 5: TPX2 overexpression rescues mitotic progression delay in KIRCs. (A) immunofluorescence localization of TPX2 and KIF15 on the mitotic spindle of fixed HeLa[EB3-GFP] (upper row) and HeLa KIRC[EB3-GFP] (lower row) cells. Tubulin was detected using the YL1/2 antibody, DNA with Hoechst 33342. Micrographs in (B) show NEB, CA, AO, and cytokinesis time points in live cells in HeLa KIRC[EB3-GFP] cells that overexpressed mCherry-TPX2 by DIC and maximum z projection mCherry fluorescence microscopy. Cells were imaged every 5 min for 90 to 190 min total. (C) Immunoblot showing relative levels of TPX2 in HeLa, HeLa KIRC-2, HeLa[EB3-GFP], and HeLa KIRC[EB3-GFP] with and without overexpression ("OE") of mCherry-TPX2. (D and E) Quantification of time needed for chromosome alignment (D) and time to anaphase onset

(E) for HeLa, HeLa KIRC-2, HeLa[EB3-GFP], and HeLa KIRC[EB3-GFP] with and without mCherry-TPX2 overexpression. Dots indicate individual cells, unfilled circles indicate mCherry-TPX2 overexpression, bars indicate mean and SD, $n = 30$ cells per group, > three biological replicates, significance was calculated by ordinary one-way ANOVA, * $p \leq 0.0306$, ** $p = 0.0036$, **** $p < 0.0001$. Scale bars, 10 μm.
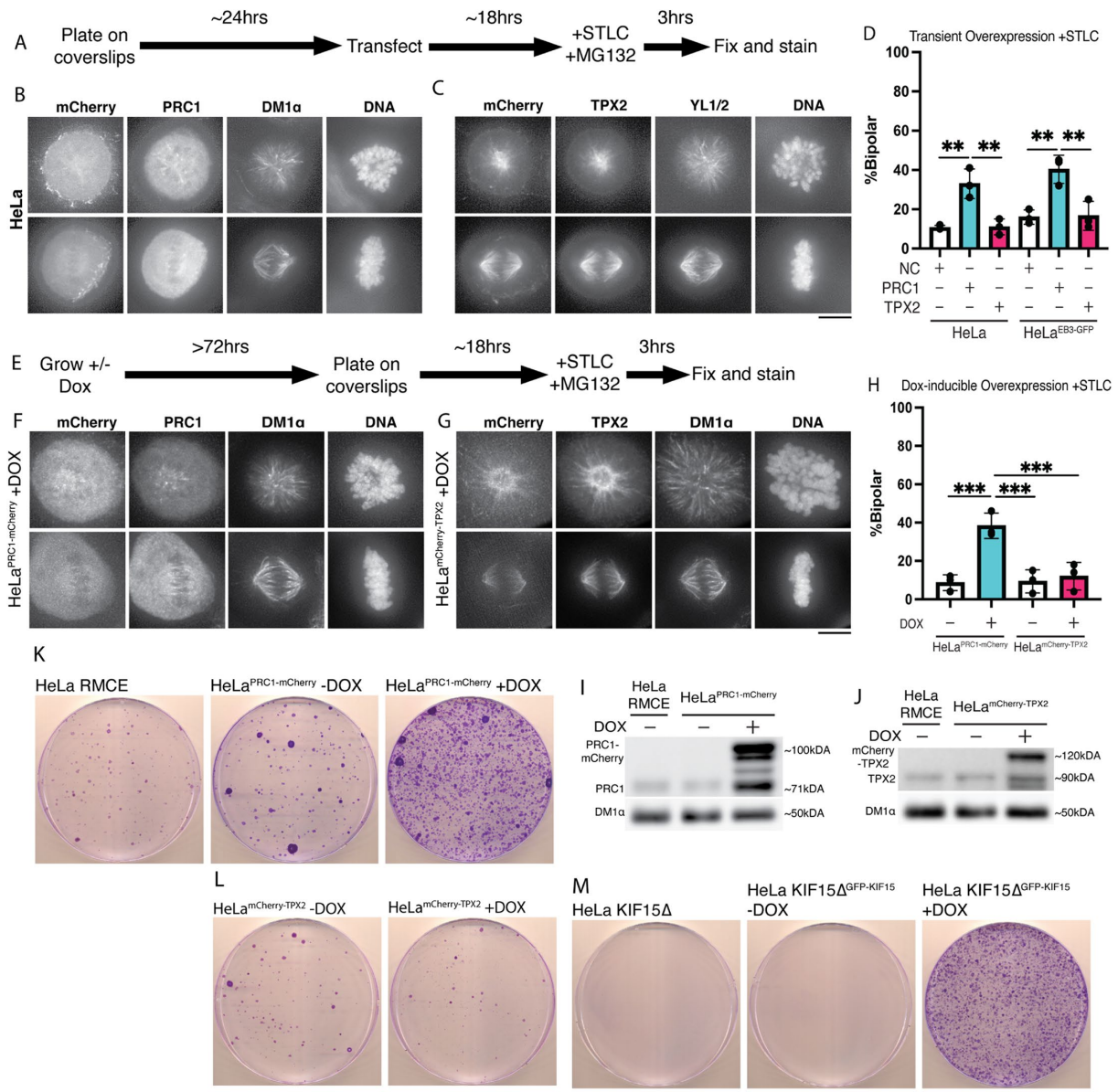
FIGURE 6: PRC1 overexpression protects against acute Eg5 inhibition and promotes the establishment of K5Is resistance. (A) Schematic of experiment corresponding to panels (B–D). Micrographs in B) and C) show representative images of monopolar (upper row) and bipolar (lower row) mitotic spindles in STLC-treated HeLa cells that overexpressed PRC1-mCherry (B) or mCherry-TPX2 (C). Tubulin was detected using DM1α (B) or YL1/2 (C), DNA with Hoechst 33342. (D) Quantification of the percentage of bipolar spindles in HeLa and HeLa^EB3-GFP cells following PRC1-mCherry or mCherry-TPX2 overexpression and 3-h treatment with STLC. Spindle morphologies were only quantified in cells that were mCherry positive. Bar graphs show mean of three biological replicates, error bard show SD, dots indicate value of each replicate, $n = 300$ per condition, statistical significance calculated by two-way ANOVA, for D. ** $p \leq 0.0073$, for H. *** $p \leq 0.0005$. (E) Schematic of experiment corresponding to panels (F–H). Micrographs in F) and G) show representative images of monopolar (upper rows) and bipolar (lower rows) mitotic spindles in STLC-treated HeLa cell lines that overexpressed PRC1-mCherry (F) or mCherry-TPX2 (G) under control of doxycycline. (H) Quantification of the percentage of bipolar spindles in HeLa^PRC1-mCherry and HeLa^mCherry-TPX2 with or without doxycycline following STLC treatment. Bar graphs show mean of three biological replicates, error bard show SD, dots indicate value of each replicate, $n = 300$ per condition, statistical significance calculated by two-way ANOVA, for D. ** $p \leq 0.0073$, for H. *** $p \leq 0.0005$. (I and J) Immunoblots showing relative levels of PRC1 (I) and TPX2 (J) upon dox-induction. Tubulin was detected using the DM1α antibody. (K) Chronic overexpression of PRC1 promotes the acquisition of HeLa cell resistance to STLC. HeLa^PRC1-mCherry cells were cultured in the absence or presence of doxycycline for 28 d, fixed, and stained with crystal violet, representative of triplicate experiment. (L) Chronic overexpression of TPX2 does not promote the acquisition of HeLa cell resistance to STLC. HeLa^mCherry-TPX2 cells were cultured in the absence or presence of doxycycline for 28 d, fixed, and stained with crystal violet, representative of triplicate experiment. (M) Chronic overexpression of KIF15 promotes the acquisition of resistance to STLC. HeLa cells that express GFP-KIF15 in a doxycycline inducible manner were cultured in the absence or presence of doxycycline for 28 d, fixed, and stained with crystal violet, representative of triplicate experiment. Scale bars (B, C, F, and G), 10 µm. Scale bars (K, L, and M), 5 cm.
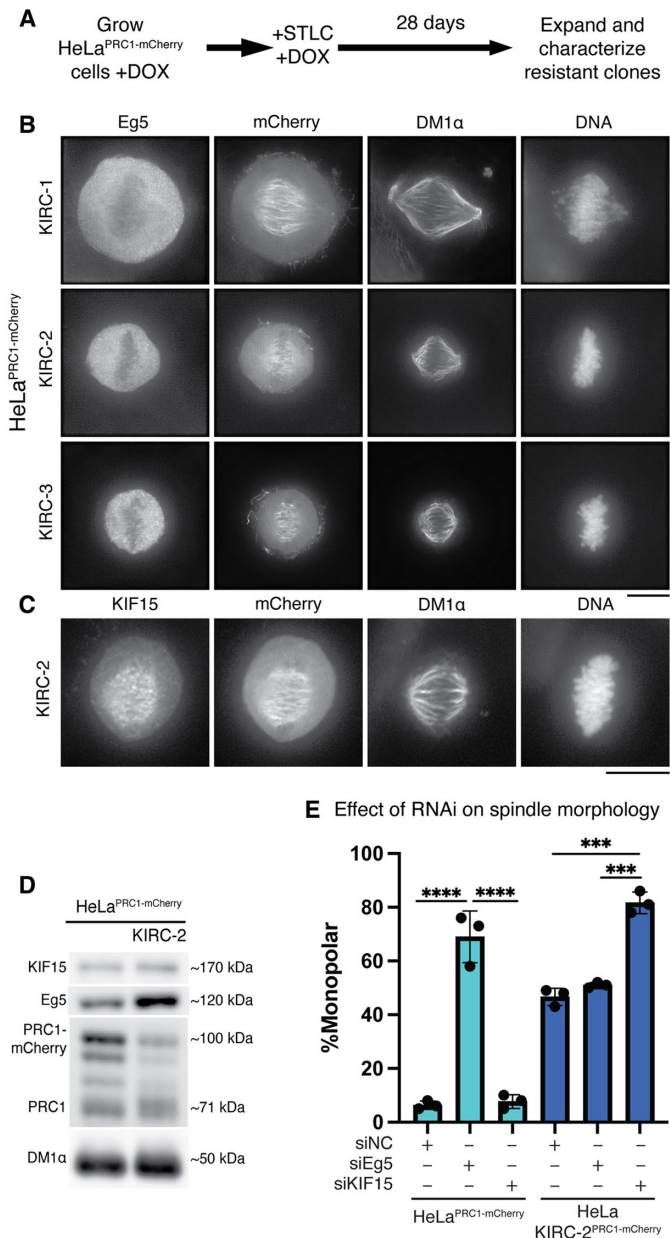
FIGURE 7: A new KIRC line that overexpresses PRC1-mCherry behaves similarly to previously described KIRCs. (A) Schematic of timeline for selection and characterization of new PRC1-mCherry overexpressing KIRC lines. Micrographs in (B) show representative images of mitotic spindles of three HeLa KIRC$^{PRC1-mCherry}$ lines stained for Eg5 and mCherry. (C) KIF15 localization on the mitotic spindle of HeLa KIRC-2$^{PRC1-mCherry}$. In all micrographs, tubulin was detected using DM1α, DNA with Hoechst 33342. Scale bars, 10 μm. (D) Immunoblots showing relative KIF15, Eg5, and PRC1 protein levels in HeLa KIRC-1^{mCherry} and HeLa KIRC-2$^{PRC1-mCherry}$, both cultured in the presence of doxycycline. (E) Quantification of the percentage of monopolar spindles following RNAi of the indicated genes. Bars show mean of three biological replicates, error bars show SD, dots indicate values of each replicate, $n = 300$ per group, statistical analysis was done using two-way ANOVA, *** $p \leq 0.0010$, **** $p < 0.0001$.

respectively – using recombination mediated cassette exchange (RMCE; Khandelia et al., 2011). Doxycycline addition induces expression of PRC1-mCherry or mCherry-TPX2, with steady state levels of proteins reaching maximal levels at 72 h. Live cell fluorescence mi-

croscopy as well as western blot confirmed that PRC1-mCherry and mCherry-TPX2 were expressed (Figure 6, I and J). We treated cells with STLC for 3 h following a 3-d induction of PRC1-mCherry or mCherry-TPX2, and processed cells for immunofluorescence using antibodies against tubulin to visualize spindle morphology (Figure 6, F and G). Results from this experiment mirrored the effects of transient PRC1 or TPX2 overexpression (Figure 6D): PRC1 protects against STLC challenge to a modest degree (HeLa$^{PRC1-mCherry}$ –DOX: 91.3% monopolar, 8.7% bipolar; HeLa$^{PRC1-mCherry}$ +DOX: 61.7% monopolar, 38.3% bipolar) whereas TPX2 does not (HeLa$^{mCherry-TPX2}$ –DOX: 90.7% monopolar, 9.3% bipolar; HeLa$^{mCherry-TPX2}$ +DOX: 88% monopolar, 12% bipolar; Figure 6H).

Persistent PRC1 overexpression promotes establishment of STLC resistance through the KIF15 spindle assembly pathway

Given that PRC1 overexpression protects spindle assembly from the effects of STLC in K5I-naïve cells, we sought to determine whether PRC1 overexpression could promote the establishment of STLC resistance. HeLa$^{PRC1-mCherry}$ cells were cultured in the presence of STLC with or without doxycycline for 28 d. Following crystal violet staining, more STLC resistant colonies emerged when cells were cultured with doxycycline – that is, with PRC1-mCherry expression "on" – as compared with HeLa$^{PRC1-mCherry}$ cells without doxycycline or to the parental HeLa RMCE acceptor line (Figure 6K). In contrast, fewer resistant colonies emerged with TPX2 overexpression after prolonged STLC treatment as compared with the effect of PRC1 overexpression (Figure 6L). Neither TPX2 nor PRC1 overexpression in HeLa KIF15Δ cell lines improved those cells' ability to establish STLC resistance (Supplemental Figure S6); no resistant colonies emerge when KIF15 is absent from cells (Figure 6M; Supplemental Figure S6) indicating that PRC1 promotes STLC resistance through a mechanism that requires KIF15.

A PRC1-mCherry overexpressing KIRC behaves similarly to HeLa and RPE-1 KIRCs

Work in yeast has demonstrated that Eg5 independent spindle assembly can be driven by the PRC1 orthologue, Ase1, in combination with a MT polymerase (Yukawa et al., 2017) or MT stabilizer (Rincon et al., 2017). Therefore, it is possible that spindle assembly in the K5I resistant HeLa$^{PRC1-mCherry}$ cells might progress through a different pathway than KIRCs previously described. To study the properties of PRC1-overexpressing KIRCs, we isolated colonies of HeLa$^{PRC1-mCherry}$ cells that survived in the presence of doxycycline and STLC for 28 d. After 28 d, colonies were isolated and expanded while continuously cultured in the presence of STLC and doxycycline (Figure 7A). Three selected KIRCs (called HeLa KIRC-1, -2, and -3$^{PRC1-mCherry}$) were screened for mitotic spindle morphology and Eg5 localization, with Eg5 being absent from the spindles of all three cell lines. HeLa KIRC-1$^{PRC1-mCherry}$ exhibited larger, more abnormal spindles while HeLa KIRC-2 and -3$^{PRC1-mCherry}$ appeared more normal (Figure 7B). HeLa KIRC-3$^{PRC1-mCherry}$ displayed very slow growth. We selected HeLa KIRC-2$^{PRC1-mCherry}$ for further analysis.

HeLa KIRC-2$^{PRC1-mCherry}$ relies on KIF15 and not Eg5 for mitotic spindle assembly, as assessed by RNAi knockdown and quantitation of spindle morphologies (Figure 7E). KIF15 is present on the mitotic spindle of HeLa KIRC-2$^{PRC1-mCherry}$ cells, while Eg5 is not (Figure 7, B and C). Upon Eg5 knockdown, HeLa KIRC-2$^{PRC1-mCherry}$ spindles are nearly evenly split between bipolar and monopolar (49% bipolar, 51% monopolar, $n = 300$) while they are predominantly monopolar upon KIF15 knockdown (18.3% bipolar, 81.7% monopolar, $n = 300$). This is in line with the characteristics of HeLa KIRC$^{EB3-GFP}$, RPE-1

KIRC-1, and HeLa KIRC-2 (Figures 2C and D, 4C). Additionally, it appears that doxycycline inducible PRC1 overexpression in HeLa[PRC1-mCherry] protects against the effect of Eg5 knockdown by RNAi similarly to its protective effect against STLC treatment in K5I naïve cells.

DISCUSSION

Although Eg5 plays a central role in spindle assembly in nearly all eukaryotic organisms, genetic and pharmacological studies in human cells have identified mechanisms that compensate for a loss of Eg5 activity. In both nontransformed and cancer cells, KIF15 is a linchpin for Eg5-independent spindle assembly (Tanenbaum *et al.*, 2009; Raaijmakers *et al.*, 2012; Sturgill and Ohi, 2013; Sturgill *et al.*, 2016; Dumas *et al.*, 2019): Overexpression of KIF15 suppresses the cytotoxicity of K5Is (Tanenbaum *et al.*, 2009; Sturgill and Ohi, 2013), whereas deletion of KIF15 prevents the emergence of KIRCs (Sturgill *et al.*, 2016). In agreement with KIF15's ability to substitute for Eg5 during spindle assembly, in vitro work has shown that KIF15 is similar to Eg5 in that it can slide antiparallel MTs apart (Reinemann *et al.*, 2017). Interestingly, glioblastoma cells can also acquire resistance to the K5I ispinesib through a mechanism that involves STAT3 phosphorylation and subsequent expression of proliferative factors, notably EGFR, and inhibition of proapoptotic cytochrome C (Kenchappa *et al.*, 2022).

While KIF15 can substitute for Eg5, KIF15 is less potent at generating centrosome separation forces, evidenced by the high monopolar index of Eg5 inhibitor resistant cells. This is likely due to differences in how KIF15 and Eg5 generate antiparallel MT sliding forces. Eg5 uses two sets of motor domains to simultaneously walk on two antiparallel MTs (Kapitein *et al.*, 2005), allowing force generated within an antiparallel overlap to scale linearly with the number of Eg5 motors (Shimamoto and Kapoor, 2018). In contrast, KIF15 associates with two antiparallel MTs using one set of motor heads and a second, nonmotile MT-binding domain (Sturgill *et al.*, 2014). Importantly, the rupture force of the nonmotile MT-binding domain is only slightly higher than the force-generating capacity of two KIF15 motors, suggesting that ensembles of >3 KIF15 motors cause motors to disengage from the overlap. We, thus, hypothesized that an antiparallel MT cross-linking factor may act synergistically with KIF15 during spindle assembly, by: 1) creating a preferred substrate for KIF15 to generate centrosome separation forces, and 2) preserving work accomplished by KIF15. In this work, we focused on PRC1 because it is the only MAP known to preferentially cross-link MTs in antiparallel. Moreover, MTs bundled by PRC1 are efficient at recruiting KIF15 in vitro (Sturgill *et al.*, 2014).

Using experimentally derived KIRCs, we find that PRC1 overexpression supports KIF15-driven spindle assembly, as demonstrated by a rescue of the delay in time to chromosome alignment and anaphase onset (Figures 3 and 4). We also demonstrate that PRC1 overexpression protects drug-naïve cells against acute exposure to a K5I. Importantly, we also show that PRC1 overexpression dramatically increases the emergence of K5I resistant cells over a long selection period (Figure 6). While PRC1 overexpression promotes the establishment of K5I resistance, PRC1 is not sufficient for spindle assembly in the absence of KIF15, indicating that KIF15 is essential for this K5I resistance pathway (Tanenbaum *et al.*, 2009; Vanneste *et al.*, 2009; Sturgill and Ohi, 2013; Ma *et al.*, 2014; Sturgill *et al.*, 2014; Dumas *et al.*, 2016; Sturgill *et al.*, 2016; Milic *et al.*, 2018; Dumas *et al.*, 2019; Solon *et al.*, 2022). Given that KIF15 is weak force-generator compared with Eg5 (Reinemann *et al.*, 2017) and evidence showing PRC1 can modulate antiparallel MT sliding based on velocity (Subramanian *et al.*, 2010; Lansky *et al.*, 2015; Gaska *et al.*, 2020;

Alfieri *et al.* 2021), we suggest that PRC1 may help to buffer opposed (inward) forces generated by dynein or the kinesin-14 HSET (Mountain *et al.*, 1999; Hentrich and Surrey, 2010). This likely contributes to the preponderance of monopolar spindles upon PRC1 depletion in KIF15-dependent cells (Figures 2 and 4).

Notably, nonmotor MT associated proteins (MAPs) have also been shown to promote Eg5 independent spindle assembly in other model organisms. In fission yeast, one Eg5-independent mitotic spindle assembly pathway relies on MT cross-linking by Ase1, an orthologue of PRC1 (Janson *et al.*, 2007; Blackwell *et al.*, 2017; Rincon *et al.*, 2017). Two additional pathways depend on kinesin-6/Klp9 or the Alp7/TACC-Alp14/TOG MT polymerase complex (Yukawa *et al.*, 2017). In plants, PRC1-related MAP65 proteins have been shown to bundle antiparallel MTs and localize to the phragmoplast after metaphase (Li *et al.*, 2017; Herrmann *et al.*, 2018).

The prominence of PRC1 proteins in Eg5 independent spindle assembly pathways begs the question of whether spindle assembly *via* non-motor MT cross-linking MAPs requires a preference for antiparallel MTs. In previous work, we showed that a subset of KIRCs (HeLa KIRC-2, KIRC-3) depend on an Eg5-rigor mutant, Eg5-G268V, a protein expected to behave as a static MT crosslinker; knockdown of Eg5 or KIF15 in these KIRCs prevents spindle assembly (Sturgill *et al.*, 2016). Because Eg5 does not exhibit a preference for parallel *versus* antiparallel MTs (Shimamoto *et al.*, 2015), it is likely that Eg5-G268V bundles MTs in both orientations (Sturgill *et al.*, 2016). Our data showing that PRC1 is also required for spindle assembly in HeLa KIRC-2 cells, suggests that an antiparallel MT bundler is also critical for KIF15-dependent spindle assembly. Currently, it is not clear whether PRC1 and Eg5-G268V provide different functions, for example, Eg5-G268V could stabilize parallel MT bundles near spindle poles whereas PRC1 stabilizes antiparallel MTs at the spindle equator. Lastly, we find that overexpression of TPX2, a MAP that would not be expected to bundle MTs in an orientation-specific manner, does not protect against acute Eg5 inhibition nor does it promote the establishment of K5I resistance (Figure 6). Interestingly, we did observe that TPX2 overexpression could rescue delays in chromosome alignment and anaphase onset in KIRCs (Figure 5). One explanation for this result could be TPX2 rescues mitotic progression in KIRCs by nucleating MTs at kinetochores (Tulu *et al.*, 2006), thereby creating more antiparallel MT overlaps at the spindle equator for KIF15 to slide apart, although the exact mechanism underlying this result remains to be fully explored.

Collectively, this work suggests that changes in spindle architecture, mediated in part by PRC1, are important for cells to switch from an Eg5 spindle assembly pathway to one driven by KIF15. By showing that PRC1 overexpression can drive K5I resistance, our work may help to improve the clinical efficacy of K5Is. Indeed, PRC1 upregulation is found in a number of cancers and is associated with poor prognosis and chromosomal instability (Li *et al.*, 2018). In a study of Ewing sarcoma, PRC1 was found to be upregulated, promoting tumor growth and indicating poor clinical outcome (Li *et al.* 2021a). Through depleting PRC1 or inhibiting its activator, Polo-like kinase (PLK) 1, Ewing sarcoma cell lines could be resensitized to chemotherapy (Li *et al.* 2021a).

MATERIALS AND METHODS

Cell culture and establishment of K5I-resistant cell lines

HeLa "Kyoto", RPE-1 *TP53*^{−/−}, and HeLa KIF15Δ (Sturgill *et al.*, 2016) cell lines were cultured in DMEM +10% fetal bovine serum (FBS) and penicillin/streptomycin. HeLa KIRC-2 (Sturgill *et al.*, 2016) and RPE-1

TP53$^{-/-}$ KIRC-1 (Dumas *et al.*, 2019) cell lines were cultured in DMEM +10% FBS and penicillin/streptomycin and 10 μM STLC (Sigma-Aldrich). HeLa$^{EB3-GFP}$ cells (Cytion) were cultured in DMEM +10% FBS and penicillin/streptomycin and 0.5 mg/ml Geneticin (G418, Life Technologies). HeLa KIRC$^{EB3-GFP}$ cells (this work) were cultured in DMEM +10% FBS, penicillin/streptomycin, 0.5 mg/ml G418 and 10 μM STLC. HeLa KIF15Δ EGFP-KIF15 cells (Sturgill *et al.*, 2016) were cultured in DMEM +10% tetracycline-characterized FBS (Cytiva), and penicillin/streptomycin.

K5I-resistant HeLa$^{EB3-GFP}$ cells were generated by growing cells to confluency in standard 15-cm dishes (Corning) and then selected in DMEM containing 10% FBS, penicillin/streptomycin, 50 mg/ml G418 and 10 μM STLC. Media was replaced roughly every other day for 28 d. On the 28th day, dishes were gently rinsed with PBS and resistant colonies were selected and expanded. Clones deemed to be useful were those that: 1) did not rely on Eg5 for passage through mitosis, 2) did rely on KIF15 to form a bipolar spindle, and 3) did not exhibit detectable amounts of Eg5 protein on the mitotic spindle. Reliance during mitosis was tested by RNAi using siRNAs described below. Eg5 localization was tested by immunostaining as described below.

HeLa RMCE and HeLa KIF15Δ RMCE cell lines (as reported in [Sturgill *et al.*, 2016]) expressing mCherry-TPX2 or PRC1-mCherry (see below) were cultured in DMEM +10% tetracycline-characterized FBS, and penicillin/streptomycin. The abilities of TPX2 and PRC1 to suppresses the cytotoxic effects of STLC was tested by induction of TPX2 or PRC1 by the addition of 2 μg/ml doxycycline (Thermo Fisher Scientific) for ~48 h and growing cells to confluency in 15-cm dishes before addition of 10 μM STLC. Cells were maintained in DMEM +10% tetracycline-characterized FBS, penicillin/streptomycin, 2 μg/ml doxycycline, and 10 μM STLC. Media was replaced approximately every other day for 28 d, at which point dishes were stained with crystal violet and imaged as described in (Sturgill *et al.*, 2016). STLC selection experiments were performed in triplicate.

RNA interference and transient transfections
Cells were plated on 12-mm acid-washed coverslips in 6-well dishes and allowed to adhere for ~24 h. siRNA transfections were performed using HiPerFect (QIAGEN) according to manufacturer's recommendations and fixed for immunostaining ~24 h after transfection. The following siRNAs were used in this study: KIF15: GGACAUAAAUUGCAAAUAC (Dharmacon), Eg5: CUGAAGACCU-GAAGACAAUdTdT (Qiagen), and PRC1: ACUCUUCUUGAAGCA-CUAUUAUUA (IDT). Control depletions were performed using All-Stars Negative Control siRNA (QIAGEN).

For plasmid transfection, cells were plated onto glass-bottom poly-D-lysine coated dishes (MatTek) or on 12-mm acid-washed coverslips in 6-well dishes and allowed to adhere for ~24 h. Plasmid transfections of 150 ng pmCherry-N1-PRC1 or 150 ng pmCherry-C1-TPX2 were performed using Lipofectamine 2000 (Invitrogen) according to manufacturer's recommendations and then fixed or used in live-cell imaging ~18 h after transfection.

Transient overexpression and STLC challenge
HeLa and HeLa$^{EB3-GFP}$ cells were plated in sixwell dishes on 12-mm acid washed coverslips and transfected with PRC1-mCherry or mCherry-TPX2 as described above. Approximately 20 h after transfection, 10 μM STLC and 10 μM MG132 (Calbiochem) were added to the culture media. Cells were fixed 3 h after addition of STLC and MG132 and processed for immunofluorescence as described below.

HeLa-RMCE transfections
Establishment of doxycycline-inducible PRC1-mCherry and mCherry-TPX2 cell lines was done using the HeLa RMCE acceptor cell line as previously described (Sturgill *et al.*, 2016). In brief, HeLa RMCE cells were grown in sixwell dishes and cotransfected 1:10 (wt/wt) with pEM784 and pEM791-mCherry-TPX2 or pEM791-PRC1-mCherry, or empty vector (negative control). ~24 h after transfection, media was replaced with selection media containing 2 μg/ml puromycin (Sigma) for 5 d and then 1 μg/ml until negative control transfected cells had died off. Emerging clones were pooled, expanded, and characterized based on mCherry-TPX2 or PRC1-mCherry expression following 2 μg/ml doxycycline treatment. Doxycycline-inducible PRC1-mCherry and mCherry-TPX2 lines were established using HeLa KIF15Δ RMCE background (Sturgill *et al.*, 2016) in the same manner.

Antibody purification and direct labeling
Full-length His6-tagged PRC1 protein was purified as described previously (Subramanian *et al.*, 2010) and used to immunize rabbits (Cocalico). Anti-PRC1 antibodies were affinity-purified by running serum over Affi-Gel 10 (Bio-Rad) coupled to PRC1 protein. Purified antibodies were dialyzed in 1xPBS, aliquoted, frozen in liquid N$_2$ and stored at –80°C.

Anti-PRC1 and anti-KIF15 antibodies were conjugated to Alexa Fluor 647 and 594, respectively, using Alexa Fluor Antibody Labeling kits (Invitrogen) and stored at –80°C.

Immunostaining, fixed- and live-cell imaging
Cells were fixed in a buffer that simultaneously permeabilizes and fixes cells (3% paraformaldehyde (Sigma-Aldrich), 100 mM K-PIPES, 10 mM K-EGTA, 1 mM MgCl$_2$, 0.2% Triton X-100) at room temperature for 10 min. Primary antibodies against PRC1 (rabbit, this study), KIF15 (rabbit, [Sturgill and Ohi, 2013]), Eg5 (rabbit, Genetex), tyrosinated α-tubulin (YL1/2; rat, Accurate Chemical), TPX2 (mouse or rabbit, Abcam), and mCherry (rat, Invitrogen) were used at 2 μg/ml for 1 h. Antirabbit, antimouse, and antirat secondary antibodies conjugated to Alexa Fluor 488, 594, or 647 (goat, Invitrogen) were used at 1:1000 dilution for 45 min. Directly labeled anti-PRC1-647 and anti-KIF15-594 antibodies were used at 2 μg/ml for 45 min and anti-DM1α-488 (mouse, Sigma-Aldrich) was used at 1:500 for 30 min. DNA was counterstained with 5 μg/ml Hoechst-33342 for 5 min.

Cells were mounted in Prolong Gold and imaged at 37°C with a DeltaVision Elite image restoration system (GE Healthcare) equipped with a 60 × 1.4 numerical aperture lens (Olympus) and a Cool SnapHQ2 charge-coupled device camera (Photometrics). Images from z-sections spaced 500-nm apart were deconvolved (Ratio [conservative], 15 iterations) with SoftWorx (GE Healthcare). Images were subsequently processed and analyzed using FIJI (ImageJ).

For live cell imaging, cells were plated onto glass-bottom poly-D-lysine coated (MatTek) dishes 24 to 48 h before imaging. Cells were imaged at 37°C in L-15 media without phenol red +10% FBS, penicillin/streptomycin, and 7 mM K-HEPES, pH = 7.7 using the DeltaVision Elite system with a 40 × 1.4 numerical aperture lens (Olympus) and DIC and fluorescence optics (FITC and/or mCherry, depending on the experimental conditions). Images were acquired every 5 min with 1-μm z-sections, utilizing image-based autofocus before each time point. Movies were then processed using ImageJ, generating maximum intensity z-projections, cropping, rotating, adjusting minimum and maximum levels and contrast.

Monopolar index and mitotic progression quantitation

Monopolar index – the percentage of monopolar spindles in a population of cells – was quantified in fixed cells following RNAi or transient overexpression of PRC1 or TPX2 and STLC challenge. For RNAi, 100 cells per coverslip for each group were counted and the number of monopolar and bipolar spindles were calculated as a percentage. For transient overexpression and STLC challenge, only the spindle morphologies of mCherry positive cells were counted. For both experiments, the average for each condition was calculated from three biological replicates for each cell background and plotted using Prism.

Mitotic progression was quantified using DIC videos from live cell imaging. The time from NEB to chromosome alignment (frame at which chromosomes of a given mitotic cell appear aligned) and from NEB to anaphase onset (frame at which chromosomes have first begun to separate) was calculated as the number of frames between each time point multiplied by the time interval between frames (#of frames x 5 min). Average time to each stage was calculated and plotted using Prism. For overexpression experiments, time to chromosome alignment and anaphase onset were only measured in transfected cells, as determined by nuclear mCherry signal at interphase and presence of fluorescence on spindle MTs during mitosis.

Molecular biology

PRC1 was inserted into pmCherry-N1 using overlapping polymerase chain reaction primers and isothermal assembly. The original pEGFP-N1-PRC1 construct was generously shared by R. Margolis (Mollinari *et al.*, 2002). The pEGFP-C1-TPX2 construct was generously shared by T. Kapoor. GFP was swapped for mCherry using overlapping PCR primers and isothermal assembly to generate pmCherry-C1-TPX2. PRC1-mCherry was inserted into pEM791 ([Khandelia *et al.*, 2011]; gift from E. Makeyev) using isothermal assembly. pEM791-mCherry-TPX2 was assembled by VectorBuilder (Chicago, IL USA). Proper assembly of each construct was confirmed by sequencing.

Protein gels and immunoblotting

To measure relative endogenous protein levels in RPE-1, KIRC-1, HeLa, KIRC-2, HeLa$^{EB3-GFP}$ and HeLa KIRC$^{EB3-GFP}$, cells were grown to confluence in standard sixwell dishes in appropriate media, washed with DPBS (Life Technologies), trypsinized and pelleted by centrifugation. To measure degree of PRC1 and TPX2 overexpression, HeLa, KIRC-2, HeLa$^{EB3-GFP}$ and HeLa KIRC$^{EB3-GFP}$ cells were grown to ~ 70% confluency in sixwell plates and transfected as previously described with pmCherry-N1-PRC1 or pmCherry-C1-TPX2. Roughly 24 h later, cells were trypsinized, washed with DPBS, and pelleted by centrifugation. To confirm PRC1-mCherry and mCherry-TPX2 induction by doxycycline in HeLa$^{PRC1-mCherry}$, HeLa KIRC-2$^{PRC1-mCherry}$, HeLa$^{mCherry-TPX2}$, cells were grown in sixwell dishes with 2 µg/ml doxycycline for 3 d, trypsinized, washed with DPBS, and pelleted by centrifugation. All cell pellets were processed in the following manner: pellets were resuspended in NP-40 buffer (10 mM sodium phosphate, pH 7.2, 150 mM NaCl, 2 mM EDTA, and 1% NP-40) with protease and phosphatase inhibitors, sonicated for 1 min, and clarified by centrifugation at 4°C for 15 min. Protein levels of each lysate were measured using Bradford reagent (Bio-Rad). Aliquots of each lysate were mixed with 5x SDS-sample dye (250 mM Tris-Cl, pH 6.8, 20% SDS, 50% glycerol, 500 mM DTT, and 500 µg/ml bromophenol blue) and boiled for 3–5 min. Samples were loaded at 10 µg total protein in a 10% SDS gel, resolved by SDS–PAGE and transferred to nitrocellulose membranes for immunoblotting.

Nitrocellulose membranes were blocked with 5% milk in PBST (1xPBS with 0.05% Tween-20) for one hour. Primary antibodies against PRC1 (rabbit, this study), KIF15 (rabbit, [Sturgill and Ohi, 2013]), KIF11 (rabbit, Proteintech), TPX2 (rabbit, Abcam), and DM1α (mouse, loading control, Sigma Aldrich) were diluted 1:1,000 (PRC1) or 1:500 (KIF15, Eg5, TPX2, DM1α) in 5% milk in PBST and incubated at 4°C overnight with rocking. Secondary IRDye 800CW goat anti-rabbit (Li-Cor) and goat antimouse Alexa Fluor 700 (Invitrogen) antibodies were diluted 1:10,000 in 5% milk in PBST and used for 1 h at room temperature with rocking. Membranes were rinsed thoroughly with PBST and imaged using an Azure Biosystems instrument.

Statistical analysis

Statistical significance was calculated by ordinary one-way or two-way ANOVA using GraphPad Prism version 10.1.0 for Mac, GraphPad Software, Boston, Massachusetts USA, www.graphpad.com.

REFERENCES

Alfieri A, Gaska I, Forth S (2021). Two modes of PRC1-mediated mechanical resistance to kinesin-driven microtubule network disruption. Curr Biol 31, 2495–2506.e4.

Baker TM, Waise S, Tarabichi M, Van Loo P (2024). Aneuploidy and complex genomic rearrangements in cancer evolution. Nat Cancer 5, 228–239.

Ben-David U, Amon A (2020). Context is everything: aneuploidy in cancer. Nat Rev Genet 21, 44–62.

Bieling P, Telley IA, Surrey T (2010). A minimal midzone protein module controls formation and length of antiparallel microtubule overlaps. Cell 142, 420–432.

Blackwell R, Edelmaier C, Sweezy-Schindler O, Lamson A, Gergely ZR, O'Toole E, Crapo A, Hough LE, McIntosh JR, Glaser MA, Betterton MD (2017). Physical determinants of bipolar mitotic spindle assembly and stability in fission yeast. Sci Adv 3, e1601603.

Cross RA, McAinsh A (2014). Prime movers: the mechanochemistry of mitotic kinesins. Nat Rev Mol Cell Biol 15, 257–271.

DeBonis S, Skoufias DA, Lebeau L, Lopez R, Robin G, Margolis RL, Wade RH, Kozielski F (2004). In vitro screening for inhibitors of the human mitotic kinesin Eg5 with antimitotic and antitumor activities. Mol Cancer Ther 3, 1079–1090.

Dumas ME, Chen GY, Kendrick ND, Xu G, Larsen SD, Jana S, Waterson AG, Bauer JA, Hancock W, Sulikowski GA, Ohi R (2019). Dual inhibition of Kif15 by oxindole and quinazolinedione chemical probes. Bioorg Med Chem Lett 29, 148–154.

Dumas ME, Sturgill EG, Ohi R (2016). Resistance is not futile: Surviving Eg5 inhibition. Cell Cycle 15, 2845–2847.

Garcia-Saez I, Skoufias DA (2021). Eg5 targeting agents: From new antimitotic based inhibitor discovery to cancer therapy and resistance. Biochem Pharmacol 184, 114364.

Gaska I, Armstrong ME, Alfieri A, Forth S (2020). The Mitotic Crosslinking Protein PRC1 Acts Like a Mechanical Dashpot to Resist Microtubule Sliding. Dev Cell 54, 367–78.e5.

Green RA, Paluch E, Oegema K (2012). Cytokinesis in animal cells. Annu Rev Cell Dev Biol 28, 29–58.

Hentrich C, Surrey T (2010). Microtubule organization by the antagonistic mitotic motors kinesin-5 and kinesin-14. J Cell Biol 189, 465–480.

Herrmann A, Livanos P, Lipka E, Gadeyne A, Hauser MT, Van Damme D, Muller S (2018). Dual localized kinesin-12 POK2 plays multiple roles during cell division and interacts with MAP65-3. EMBO Rep 19, e46085.

Izquierdo D, Wang WJ, Uryu K, Tsou MF (2014). Stabilization of cartwheel-less centrioles for duplication requires CEP295-mediated centriole-to-centrosome conversion. Cell Rep 8, 957–965.

Jagric M, Risteski P, Martincic J, Milas A, Tolic IM (2021). Optogenetic control of PRC1 reveals its role in chromosome alignment on the spindle by overlap length-dependent forces. eLife 10, e61170.

Janson ME, Loughlin R, Loiodice I, Fu C, Brunner D, Nedelec FJ, Tran PT (2007). Crosslinkers and motors organize dynamic microtubules to form stable bipolar arrays in fission yeast. Cell 128, 357–368.

Janssen A, Medema RH (2011). Mitosis as an anti-cancer target. Oncogene 30, 2799–2809.

Jordan MA, Thrower D, Wilson L (1992). Effects of vinblastine, podophyllotoxin and nocodazole on mitotic spindles. Implications for the role of microtubule dynamics in mitosis. J Cell Sci 102 (Pt 3), 401–416.

Kajtez J, Solomatina A, Novak M, Polak B, Vukusic K, Rudiger J, Cojoc G, Milas A, Sumanovac Sestak I, Risteski P, et al. (2016). Overlap microtubules link sister k-fibres and balance the forces on bi-oriented kinetochores. Nat Commun 7, 10298.

Kapitein LC, Peterman EJ, Kwok BH, Kim JH, Kapoor TM, Schmidt CF (2005). The bipolar mitotic kinesin Eg5 moves on both microtubules that it crosslinks. Nature 435, 114–118.

Kapoor TM (2017). Metaphase Spindle Assembly. Biology 6, 8.

Kapoor TM, Mayer TU, Coughlin ML, Mitchison TJ (2000). Probing spindle assembly mechanisms with monastrol, a small molecule inhibitor of the mitotic kinesin, Eg5. J Cell Biol 150, 975–988.

Kenchappa RS, Dovas A, Argenziano MG, Meyer CT, Stopfer LE, Banu MA, Pereira B, Griffith J, Mohammad A, Talele S, et al. (2022). Activation of STAT3 through combined SRC and EGFR signaling drives resistance to a mitotic kinesin inhibitor in glioblastoma. Cell Rep 39, 110991.

Khandelia P, Yap K, Makeyev EV (2011). Streamlined platform for short hairpin RNA interference and transgenesis in cultured mammalian cells. Proc Natl Acad Sci USA 108, 12799–12804.

Kurasawa Y, Earnshaw WC, Mochizuki Y, Dohmae N, Todokoro K (2004). Essential roles of KIF4 and its binding partner PRC1 in organized central spindle midzone formation. EMBO J 23, 3237–3248.

Lansky Z, Braun M, Ludecke A, Schlierf M, ten Wolde PR, Janson ME, Diez S (2015). Diffusible crosslinkers generate directed forces in microtubule networks. Cell 160, 1159–1168.

Li H, Sun B, Sasabe M, Deng X, Machida Y, Lin H, Julie Lee YR, Liu B (2017). Arabidopsis MAP65-4 plays a role in phragmoplast microtubule organization and marks the cortical cell division site. New Phytol 215, 187–201.

Li J, Dallmayer M, Kirchner T, Musa J, Grunewald TGP (2018). PRC1: Linking Cytokinesis, Chromosomal Instability, and Cancer Evolution. Trends Cancer 4, 59–73.

Li J, Ohmura S, Marchetto A, Orth MF, Imle R, Dallmayer M, Musa J, Knott MML, Holting TLB, Stein S, et al. (2021a). Therapeutic targeting of the PLK1-PRC1-axis triggers cell death in genomically silent childhood cancer. Nat Commun 12, 5356.

Li XH, Ju JQ, Pan ZN, Wang HH, Wan X, Pan MH, Xu Y, Sun MH, Sun SC (2021b). PRC1 is a critical regulator for anaphase spindle midzone assembly and cytokinesis in mouse oocyte meiosis. FEBS J 288, 3055–3067.

Ma HT, Erdal S, Huang S, Poon RY (2014). Synergism between inhibitors of Aurora A and KIF11 overcomes KIF15-dependent drug resistance. Mol Oncol 8, 1404–1418.

Matkovic J, Ghosh S, Cosic M, Eibes S, Barisic M, Pavin N, Tolic IM (2022). Kinetochore- and chromosome-driven transition of microtubules into bundles promotes spindle assembly. Nat Commun 13, 7307.

Mayer TU, Kapoor TM, Haggarty SJ, King RW, Schreiber SL, Mitchison TJ (1999). Small molecule inhibitor of mitotic spindle bipolarity identified in a phenotype-based screen. Science 286, 971–974.

McIntosh JR, Hepler PK, Van Wie DG (1969). Model for Mitosis. Nature 224, 659–663.

Milic B, Chakraborty A, Han K, Bassik MC, Block SM (2018). KIF15 nanomechanics and kinesin inhibitors, with implications for cancer chemotherapeutics. Proc Natl Acad Sci USA 115, E4613–E4622.

Mitchison T, Kirschner M (1984). Dynamic instability of microtubule growth. Nature 312, 237–242.

Mollinari C, Kleman JP, Jiang W, Schoehn G, Hunter T, Margolis RL (2002). PRC1 is a microtubule binding and bundling protein essential to maintain the mitotic spindle midzone. J Cell Biol 157, 1175–1186.

Mountain V, Simerly C, Howard L, Ando A, Schatten G, Compton DA (1999). The kinesin-related protein, HSET, opposes the activity of Eg5 and cross-links microtubules in the mammalian mitotic spindle. J Cell Biol 147, 351–366.

Oriola D, Needleman DJ, Brugues J (2018). The Physics of the Metaphase Spindle. Annu Rev Biophys 47, 655–673.

Orth JD, Tang Y, Shi J, Loy CT, Amendt C, Wilm C, Zenke FT, Mitchison TJ (2008). Quantitative live imaging of cancer and normal cells treated with Kinesin-5 inhibitors indicates significant differences in phenotypic responses and cell fate. Mol Cancer Ther 7, 3480–3489.

Ota T, Suzuki Y, Nishikawa T, Otsuki T, Sugiyama T, Irie R, Wakamatsu A, Hayashi K, Sato H, Nagai K, et al. (2004). Complete sequencing and characterization of 21,243 full-length human cDNAs. Nature Genetics 36, 40–45.

Petry S (2016). Mechanisms of Mitotic Spindle Assembly. Annu Rev Biochem 85, 659–683.

Polak B, Risteski P, Lesjak S, Tolic IM (2017). PRC1-labeled microtubule bundles and kinetochore pairs show one-to-one association in metaphase. EMBO Rep 18, 217–230.

Raaijmakers JA, van Heesbeen RG, Meaders JL, Geers EF, Fernandez-Garcia B, Medema RH, Tanenbaum ME (2012). Nuclear envelope-associated dynein drives prophase centrosome separation and enables Eg5-independent bipolar spindle formation. EMBO J 31, 4179–4190.

Rath O, Kozielski F (2012). Kinesins and cancer. Nat Rev Cancer 12, 527–539.

Reinemann DN, Sturgill EG, Das DK, Degen MS, Voros Z, Hwang W, Ohi R, Lang MJ (2017). Collective Force Regulation in Anti-parallel Microtubule Gliding by Dimeric Kif15 Kinesin Motors. Curr Biol 27, 2810–2820.e6.

Renda F, Miles C, Tikhonenko I, Fisher R, Carlini L, Kapoor TM, Mogilner A, Khodjakov A (2022). Non-centrosomal microtubules at kinetochores promote rapid chromosome biorientation during mitosis in human cells. Curr Biol 32, 1049–1063.e4.

Rincon SA, Lamson A, Blackwell R, Syrovatkina V, Fraisier V, Paoletti A, Betterton MD, Tran PT (2017). Kinesin-5-independent mitotic spindle assembly requires the antiparallel microtubule crosslinker Ase1 in fission yeast. Nat Commun 8, 15286.

Rowinsky EK, Cazenave LA, Donehower RC (1990). Taxol: a novel investigational antimicrotubule agent. J Natl Cancer Inst 82, 1247–1259.

Sansregret L, Swanton C (2017). The Role of Aneuploidy in Cancer Evolution. Cold Spring Harb Perspect Med 7, a028373.

Sawin KE, LeGuellec K, Philippe M, Mitchison TJ (1992). Mitotic spindle organization by a plus-end-directed microtubule motor. Nature 359, 540–543.

Shi J, Orth JD, Mitchison T (2008). Cell type variation in responses to antimitotic drugs that target microtubules and kinesin-5. Cancer Res 68, 3269–3276.

Shimamoto Y, Forth S, Kapoor TM (2015). Measuring Pushing and Braking Forces Generated by Ensembles of Kinesin-5 Crosslinking Two Microtubules. Dev Cell 34, 669–681.

Shimamoto Y, Kapoor TM (2018). Analyzing the micromechanics of the cell division apparatus. Methods Cell Biol 145, 173–190.

Skoufias DA, DeBonis S, Saoudi Y, Lebeau L, Crevel I, Cross R, Wade RH, Hackney D, Kozielski F (2006). S-trityl-L-cysteine is a reversible, tight binding inhibitor of the human kinesin Eg5 that specifically blocks mitotic progression. J Biol Chem 281, 17559–17569.

Solon AL, Zaniewski TM, O'Brien P, Clasby M, Hancock WO, Ohi R (2022). Synergy between inhibitors of two mitotic spindle assembly motors undermines an adaptive response. Mol Biol Cell 33, ar132.

Sturgill EG, Das DK, Takizawa Y, Shin Y, Collier SE, Ohi MD, Hwang W, Lang MJ, Ohi R (2014). Kinesin-12 Kif15 targets kinetochore fibers through an intrinsic two-step mechanism. Curr Biol 24, 2307–2313.

Sturgill EG, Norris SR, Guo Y, Ohi R (2016). Kinesin-5 inhibitor resistance is driven by kinesin-12. J Cell Biol 213, 213–227.

Sturgill EG, Ohi R (2013). Kinesin-12 differentially affects spindle assembly depending on its microtubule substrate. Curr Biol 23, 1280–1290.

Subramanian R, Wilson-Kubalek EM, Arthur CP, Bick MJ, Campbell EA, Darst SA, Milligan RA, Kapoor TM (2010). Insights into antiparallel microtubule crosslinking by PRC1, a conserved nonmotor microtubule binding protein. Cell 142, 433–443.

Tanenbaum ME, Macurek L, Janssen A, Geers EF, Alvarez-Fernandez M, Medema RH (2009). Kif15 cooperates with eg5 to promote bipolar spindle assembly. Curr Biol 19, 1703–1711.

Toso RJ, Jordan MA, Farrell KW, Matsumoto B, Wilson L (1993). Kinetic stabilization of microtubule dynamic instability in vitro by vinblastine. Biochemistry 32, 1285–1293.

Tulu US, Fagerstrom C, Ferenz NP, Wadsworth P (2006). Molecular requirements for kinetochore-associated microtubule formation in mammalian cells. Curr Biol 16, 536–541.

Valdez VA, Neahring L, Petry S, Dumont S (2023). Mechanisms underlying spindle assembly and robustness. Nat Rev Mol Cell Biol 24, 523–542.

Vanneste D, Takagi M, Imamoto N, Vernos I (2009). The role of Hklp2 in the stabilization and maintenance of spindle bipolarity. Curr Biol 19, 1712–1717.

Wittmann T, Wilm M, Karsenti E, Vernos I (2000). TPX2, A novel xenopus MAP involved in spindle pole organization. J Cell Biol 149, 1405–1418.

Yukawa M, Kawakami T, Okazaki M, Kume K, Tang NH, Toda T (2017). A microtubule polymerase cooperates with the kinesin-6 motor and a microtubule cross-linker to promote bipolar spindle assembly in the absence of kinesin-5 and kinesin-14 in fission yeast. Mol Biol Cell 28, 3647–3659.

Zhang D, Kanakkanthara A (2020). Beyond the Paclitaxel and Vinca Alkaloids: Next Generation of Plant-Derived Microtubule-Targeting Agents with Potential Anticancer Activity. Cancers (Basel) 12, 1721.